

Article

# Antimicrobial Nanostructured Bioactive Coating Based on Fe<sub>3</sub>O<sub>4</sub> and Patchouli Oil for Wound Dressing

Marius Rădulescu <sup>1</sup>, Ecaterina Andronescu <sup>2</sup>, Alina Maria Holban <sup>2,3,4</sup>, Bogdan Stefan Vasile <sup>2</sup>, Florin Iordache <sup>5</sup>, Laurențiu Mogoantă <sup>6</sup>, George Dan Mogoșanu <sup>7</sup>, Alexandru Mihai Grumezescu <sup>2,\*</sup>, Mihaela Georgescu <sup>3,4</sup> and Mariana Carmen Chifiriuc <sup>3,4</sup>

<sup>1</sup> Department of Inorganic Chemistry, Physical Chemistry and Electrochemistry, Faculty of Applied Chemistry and Materials Science, University Politehnica of Bucharest, 1–7 Polizu Street, Bucharest 011061, Romania; radulescu\_marius@yahoo.com

<sup>2</sup> Department of Science and Engineering of Oxide Materials and Nanomaterials, Faculty of Applied Chemistry and Materials Science, University Politehnica of Bucharest, 1–7 Polizu Street, Bucharest 011061, Romania; ecaterina.andronescu@upb.ro (E.A.); alina\_m\_h@yahoo.com (A.M.H.); bogdan.vasile@upb.ro (B.S.V.)

<sup>3</sup> Microbiology Immunology Department, Faculty of Biology, University of Bucharest, 1–3 Portocalelor Lane, Sector 5, Bucharest 77206, Romania; georgescumihaela@gmail.com (M.G.); carmen\_balotescu@yahoo.com (M.C.C.)

<sup>4</sup> Research Institute of the University of Bucharest -ICUB: Life, Environmental and Earth Sciences, Spl. Independentei 91–95, Bucharest 0500088, Romania

<sup>5</sup> Department of Fetal and Adult Stem Cell Therapy, Institute of Cellular Biology and Pathology of Romanian Academy, 8, B.P. Hasdeu, Bucharest 050568, Romania; floriniordache84@yahoo.com

<sup>6</sup> Research Center for Microscopic Morphology and Immunology, University of Medicine and Pharmacy of Craiova, Petru Rares Street, No. 2, Craiova 200349, Romania; editor@rjme.ro

<sup>7</sup> Department of Pharmacognosy & Phytotherapy, Faculty of Pharmacy, University of Medicine and Pharmacy of Craiova, Petru Rares Street, No. 2, Craiova 200349, Romania; mogosanu2006@yahoo.com

\* Correspondence: grumezescu@yahoo.com; Tel.: +40-21-402-3960

Academic Editor: Hugo F. Lopez

Received: 8 March 2016; Accepted: 26 April 2016; Published: 30 April 2016

**Abstract:** The aim of this study was to develop a biocompatible coating for wound dressings, containing iron oxide nanoparticles functionalized with patchouli essential oil in order to obtain improved antimicrobial properties able to prevent biofilm development and consecutive associated infections. The bioactive coating was prepared by the co-precipitation of a precursor in an alkaline solution of patchouli oil. The prepared surface was characterized by XRD (X ray diffraction), TEM (transmission electron microscopy), SAED (selected area diffraction), SEM (scanning electron microscopy) and FT-IR (Fourier transform infrared spectroscopy). The bioevaluation of the obtained coating consisted in antimicrobial, as well as *in vitro* and *in vivo* biocompatibility and biodistribution assays. The obtained coating revealed a strong anti-biofilm activity maintained up to 72 h, as well as a low cytotoxicity on mammalian cells and a good biodistribution after intraperitoneal injection in mice. These results demonstrate the promising potential of the respective coatings for the management of wound infections and for the development of soft materials with improved resistance to microbial colonization.

**Keywords:** patchouli oil; wound dressing; magnetite; nanostructured surfaces

## 1. Introduction

Wound infections are commonly caused by microbial biofilms developed on the damaged tissues, which due to the pro-inflammatory induced response delay the normal progression of healing requiring

longer periods of care and more complex treatment regimens, thus increasing the treatment cost and negatively impact the life quality of the affected patients [1–3]. Selection of the appropriate wound dressing is important for correcting the underlying causes of non-healing wounds, such as biofilms development and in this context, novel technological solutions in the design of improved dressings for the wound management are required [4]. The incorporation of natural compounds with antimicrobial activity, which prevent or treat wound infections may aid tissue regeneration. It has been already well established that many plants or plant-derived compounds (such as usnic acid [5], eugenol, cinnamaldehyde [6], limonene [7] *etc.*) exhibit wound healing activities and are used in the design of bioactive wound dressings. Moreover, this could be a valuable approach in the particular context of the global emergence of antibiotic resistance phenomenon. Essential oils are an interesting alternative to current antibiotics, as the possibility of bacteria developing resistance is lower, due to their multiple mechanisms of action and targets [8–10]. However, due to their high volatility, reaching the desired therapeutic effect requires the use of appropriate carriers [11].

Magnetite is one of the most used inorganic nanomaterials for variable biomedical, both clinical and research applications, including the development of novel antimicrobial strategies, due to their good biocompatibility [12] and intrinsic antimicrobial properties, as well as their quality to act in synergy with other antimicrobial drugs (such as antibiotics but also natural products that may have antimicrobial effects, such as plant-derived compounds and essential oils) or to act as effective drug carriers [13–15].

The purpose of this study was to obtain and bioevaluate a novel wound dressing coating, based on iron oxide nanoparticles and patchouli essential oil (PAT), with good biocompatibility and improved antimicrobial activity.

## 2. Results

Analysis through powder X-ray diffraction (Figure 1) was carried out to confirm the crystalline nature of the magnetite nanoparticles coated with PAT. The XRD pattern may be indexed based on the face centered cubic structure of magnetite (JCPDS file No. 19-0629). This confirmed that the magnetite particles coated with PAT were in the form of nanocrystals, as evidenced by the peaks at  $2\theta$  values of  $30.79^\circ$ ,  $36.32^\circ$ ,  $43.55^\circ$ ,  $54.62^\circ$ ,  $56.87^\circ$  and  $63.10^\circ$  corresponding to (220), (311), (400), (422), (511) and (440) Bragg's reflections, corresponding to the face centered cubic (fcc) structures of magnetite. By using Debye-Scherrer equation,  $D = 0.89 \cdot \lambda / \beta \cdot \cos\theta$ , where  $D$  is the average grain size,  $\lambda$  is the X-ray wavelength (0.15405 nm),  $\theta$  and  $\beta$  are the diffraction angle and FWHM of an observed peak, respectively, we have estimated the average crystallite size for  $\text{Fe}_3\text{O}_4$  as 7.1 nm. The strongest peak (311) at  $2\theta = 36.32^\circ$  was used to calculate the average crystallite size ( $D$ ) of  $\text{Fe}_3\text{O}_4$  particles.

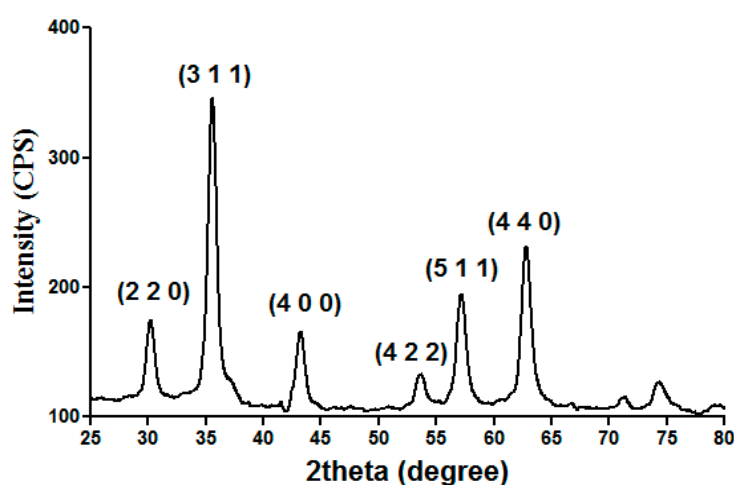
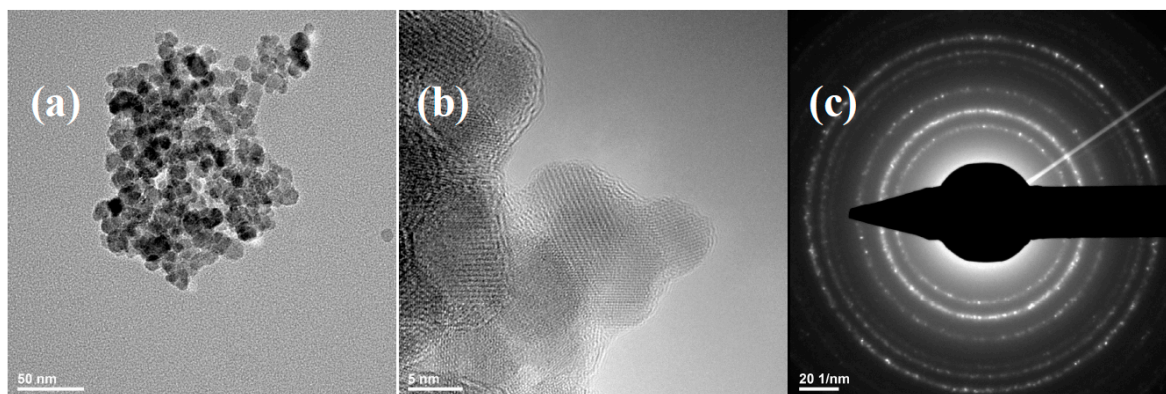


Figure 1. X ray diffraction (XRD) pattern of  $\text{Fe}_3\text{O}_4$ @PAT.

The morphology of the magnetite nanoparticles coated with PAT has been investigated by TEM. Figure 2 presents the TEM and HR-TEM images and SAED pattern of  $\text{Fe}_3\text{O}_4\text{@PAT}$ . It can be clearly seen from TEM images that nanoparticles are nearly spherical with an average diameter of 7.5 nm, which is in concordance with the results obtained from XRD. The particles are presented as clusters with tendency to form agglomerates. From the SAED pattern, it can be concluded the magnetite is the single crystalline phase.



**Figure 2.** Transmission electron microscopy (TEM) image (a), HR-TEM (high resolution electron microscopy) image (b) and SAED (selected area diffraction) pattern (c) of  $\text{Fe}_3\text{O}_4\text{@PAT}$ .

The modified wound dressing was characterized by SEM and TEM in order to confirm the presence of magnetite nanoparticles on the surface. According to Figure 3, it can be seen that the textile fibers are coated with magnetite nanoparticles. The nanoparticles are distributed on the entire surface of the wound dressing fibers, but at higher magnification it can be seen aggregates of  $\text{Fe}_3\text{O}_4\text{@PAT}$ . In Figure 4, TEM images of modified wound dressings are plotted. It can be seen that the thickness of deposited layer is irregular, varying from 5 nm to 15 nm. Also, in the co-precipitation process of magnetite nanoparticles on the surface of wound dressing, magnetite nanoparticles did not lose their crystallinity (Figure 4).

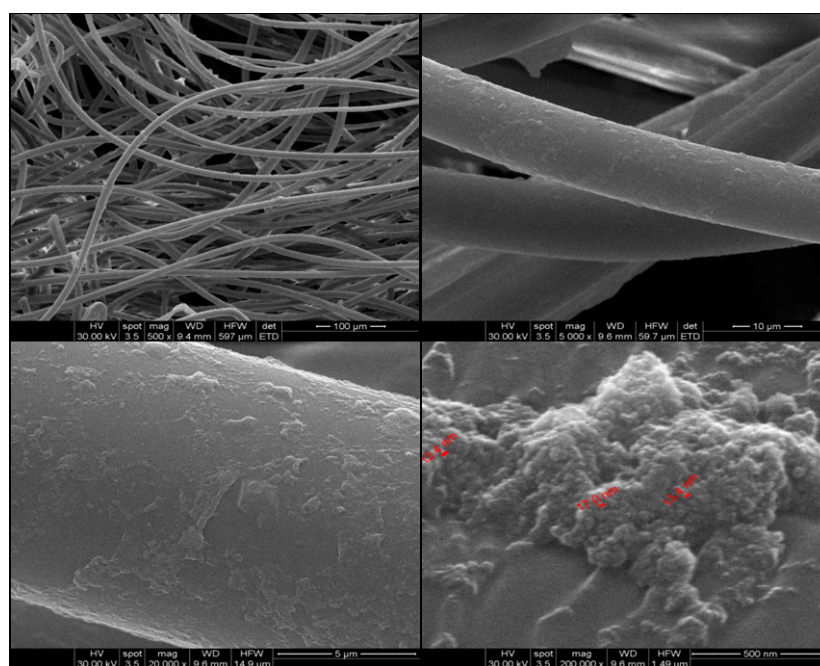


**Figure 3.** SEM images of coated wound dressing.

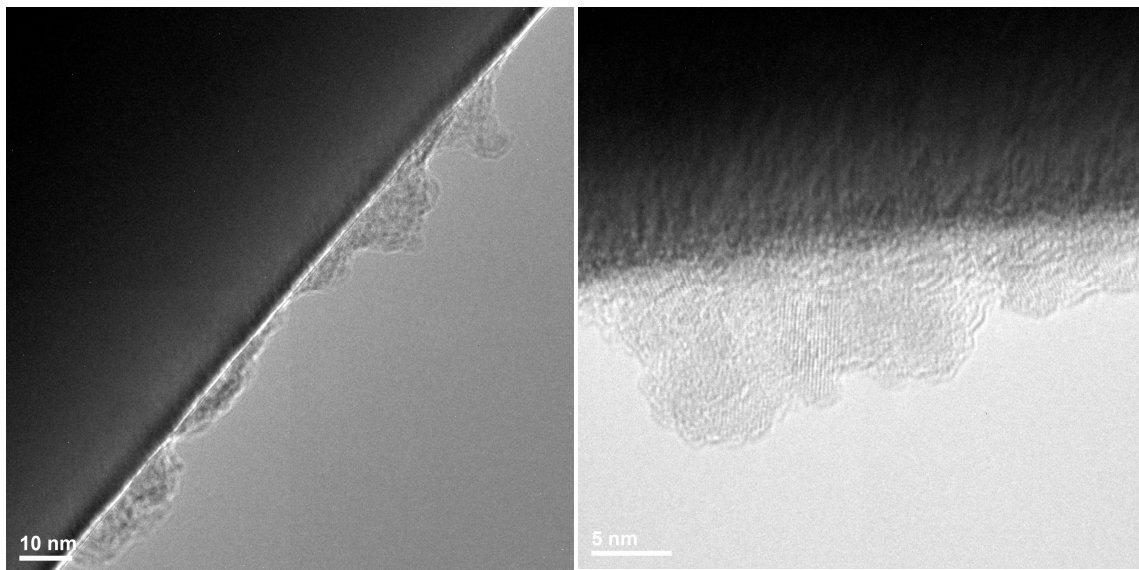


**Figure 4.** TEM images of coated wound dressing.

The biological evaluation of the obtained coated surfaces regarding their biocompatibility was tested both *in vitro*, on cultured human cells, but also *in vivo*, using a mouse model. The *in vitro* results demonstrated that the obtained coatings are biocompatible, allowing the normal development and growth of the EAhy926 endothelial cell line. The monolayer developed on coated surfaces exhibited a normal morphology, similar to the aspect of the cells developed on bare substratum (Figure 5).

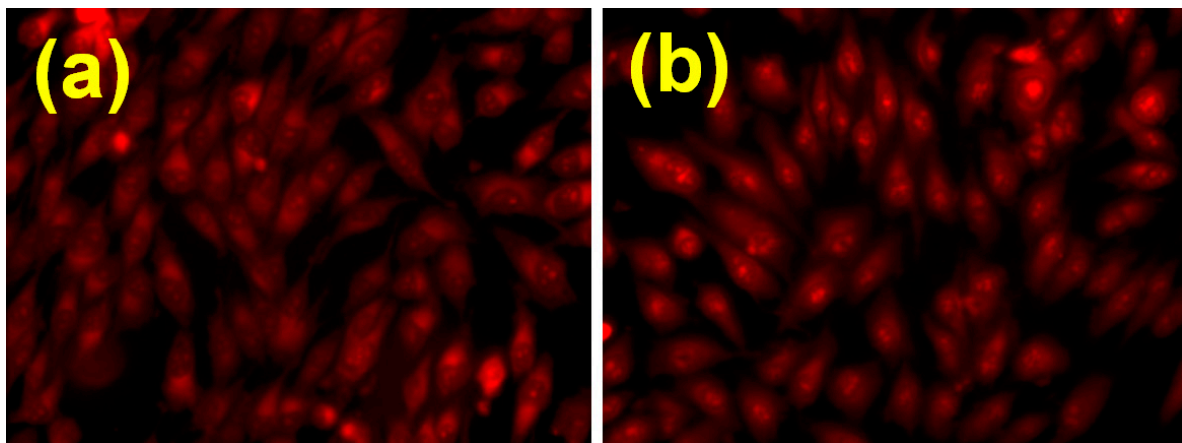


**Figure 5.** Human endothelial cells (EAhy926 cell line) after 72 h of growth on control (a) and coated surfaces (b).

The *in vivo* results revealed that the obtained nanostructures do not form clusters in most of the investigated vital organs, being absent in the brain, liver, myocardium, pancreas and kidney. Small brown nanoparticles clusters were observed in the red pulp of the spleen, being also engulfed by macrophages at that level. In the lungs, very low amounts of nanoparticles were observed 7 days after treatment (Figure 6).

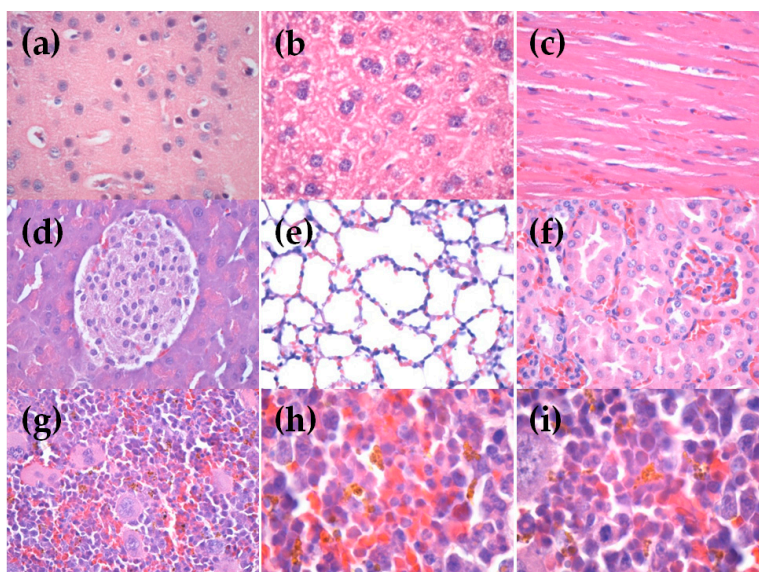


**Figure 6.** Cross-section of  $\text{Fe}_3\text{O}_4\text{@PAT}$  nanoparticles treated mouse brain (a), liver (b), myocardium (c), pancreas (d), lung (e), kidney (f), spleen (g–i). Collected sample after 7 days. Nanoparticles were observed only in the red pulp. Hematoxylin-Eosin staining (HE):  $\times 400$  (a–g);  $\times 1000$  (h,i).

The nanoparticles functionalized with PAT were absent in the brain, as well as in the liver, myocardium, pancreas, lung and kidney after 14 of administration (Figure 7). In exchange, in the spleen, the functionalized nanoparticles were found only in the red pulp in a concentration higher than in samples taken after 7 days and were absent in the white pulp. However, in the white pulp we observed hypertrophy due to the fact that nanoparticles stimulated the formation of macrophages with multilobular nucleus. In the red pulp, the nanoparticles were found in the macrophages from both Billroth cords and the capillaries and sinusoids. The nanoparticles have been evidenced as brown-blackish, granular, spherical agglomerates of varying size, with a diameter of up to  $3\ \mu\text{m}$ . The density of the endocytosed nanoparticles varied from one cell to another (Figure 7).

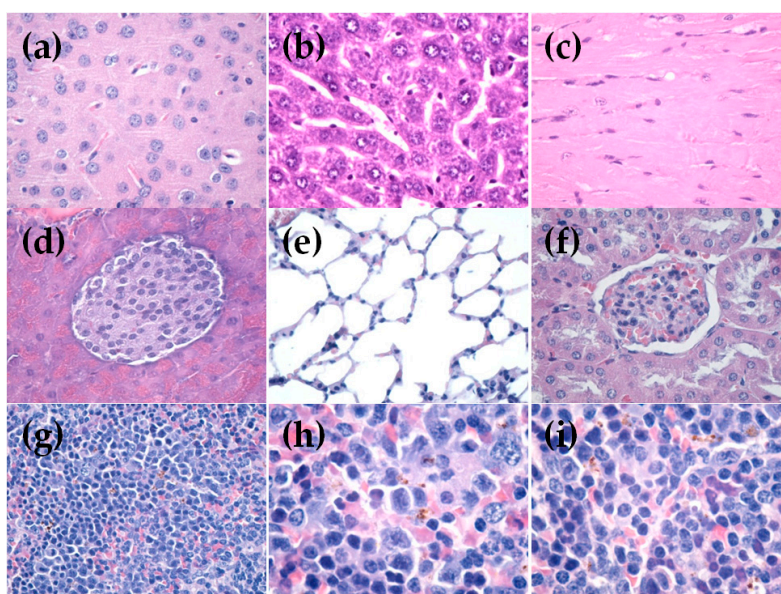


**Figure 7.** Cross-section of  $\text{Fe}_3\text{O}_4\text{@PAT}$  nanoparticles treated mouse brain (a), liver (b), myocardium (c), pancreas (d), lung (e), kidney (f), spleen (g–i). Collected samples after 14 days. Nanoparticles were observed only in the red pulp. Hematoxylin-Eosin staining (HE):  $\times 400$  (a–g);  $\times 1000$  (h,i).

These results reveal that the obtained nanoparticles could be efficiently used for developing optimized wound dressings. Also, since they are not cytotoxic *in vivo* and have a good biodistribution in terms that do not form clusters into the vital organs, these nanoparticles may be good candidates for the design of improved medical surfaces and devices with tailored properties, which do not harm the host body after their detachment from the surface of the implanted device, for example [16].

The antimicrobial activity results have shown an efficient inhibition of the *S. aureus* biofilm development, after 24 and 48 h incubation in the presence of the obtained bioactive coatings, as revealed by the decrease with at least 2 logs of the number of viable biofilm embedded cells developed on the coated glass slides, as compared to uncoated glass slides used as controls (Figure 8). Only a slight anti-biofilm effect was also recorded against the 72 h biofilms, probably due to the increased amount of the biofilm protective matrix, on one hand, and to the consumption of the incorporated essential oil, on the other one.

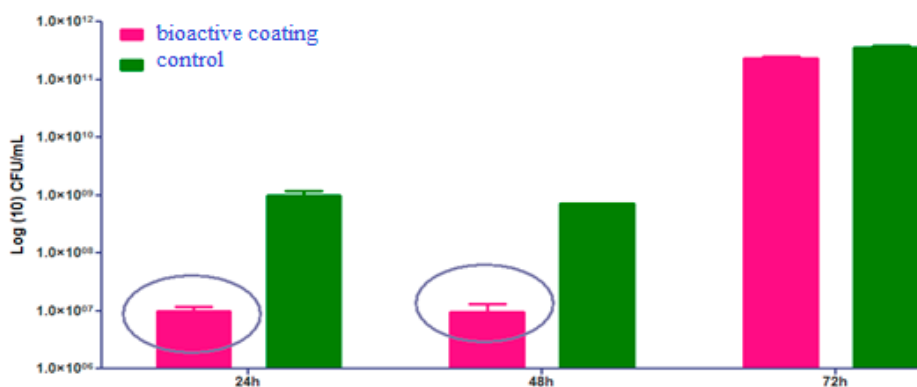


**Figure 8.** Graphic representation of the number of *S. aureus* biofilm embedded viable cells ( $\log_{10}$ CFU (colony forming units)/mL) harvested from the coated (bioactive coating) and uncoated control.

These observations suggest that the coatings could be utilized for up to 72 h, but for a safe and efficient treatment it would be recommended to replace the dressing each 24 h.

### 3. Discussion

*S. aureus* is a component of resident human microbiota of 20%–80% of human population, which is transitory or permanently colonized with these Gram-positive cocci in their upper respiratory tract [17]. The nasal carriage provides a permanent risk for the dissemination of *S. aureus* in other areas of the body or for contamination of the environment and further, of immunodepressed patients, in which cases a staphylococcal infection could occur [18]. The virulence of this opportunistic pathogen is amplified by its multiple drug resistance and ability to form multilayered biofilms, which are responsible for persistent, chronic and recurrent infections. As a nosocomial opportunistic pathogen, *S. aureus* is one of the most frequently encountered etiological agents of different wound (surgical, pressure ulcers, diabetic ulcers, or hospital- or community-acquired injuries) infections [19,20]. Bacterial colonization of wounds can increase wound severity and interfere with healing [21]. Previous studies have confirmed that the modification of absorbent dressings with essential oils led to better therapeutic results, consecutive to the enhanced antimicrobial protection [22–24]. In the review of Sevgi *et al.*, the essential oils from *Matricaria chamomilla* and tea tree as well as the extracts from *Bulbine frutescens*, *Eremophila longifolia* and *Tamarindus indica* are cited as useful alternatives for the treatment wounds treatment, due to their bactericidal properties, but also to the cicatrizing, anti-oxidant and anti-inflammatory activities [25]. PAT has been previously demonstrated to be very active against *S. aureus* strains, the most potent antimicrobial compounds being pogostone and (–)-*patchouli* alcohol [26]. In the present study we demonstrated the inhibitory effect of the

bioactive nanostructured coating based on magnetite and PAT against the *S. aureus* biofilm initiation and development.

## 4. Materials and Method

### 4.1. Materials

All chemicals used in the experiments were of analytical reagent grade and were used without further purification.

### 4.2. Fabrication of Nanoparticles and Preparation of Modified Wound Dressing

Functionalized magnetite nanoparticles was prepared by co-precipitation according to our published paper [27]. In the present paper, 500  $\mu\text{L}$  of PAT was dispersed in 200 mL of distilled-deionized water, under stirring conditions. Then, 6 mL of 25%  $\text{NH}_4\text{OH}$  solution (13.4 M) was added to the PAT solution. Thereafter, a 200 mL solution, consisting of  $\text{FeCl}_3$  and  $\text{FeSO}_4$  in molar ratio (2:1) was dropped under permanent stirring, leading to the formation of a black precipitate. In order to obtain the modified wound dressing, the procedure was similar. In the basic aqueous solution of PAT were added wound dressing (rayon/polyester) sections (1  $\text{cm}^2$ ) aseptically cut and after that the  $\text{Fe}^{2+}$  and  $\text{Fe}^{3+}$  ions were added dropwise. After complete addition of  $\text{Fe}^{3+}$  and  $\text{Fe}^{2+}$  the sections of wound dressings were washed with distilled-deionized water for 3 times and dried for physic-chemical characterization, *in vitro* and *in vivo* experiments.

### 4.3. Characterization Methods

#### 4.3.1. XRD

X-ray diffraction analysis was performed on a Shimadzu XRD 6000 diffractometer (Shimadzu, Kyoto, Japan,) at room temperature. In all the cases, Cu  $\text{K}\alpha$  radiation from a Cu X-ray tube (run at 15 mA and 30 kV) was used. The samples were scanned in the Bragg-Brentano geometry with  $2\theta$  angle range of  $20^\circ$ – $80^\circ$ .

#### 4.3.2. TEM

The transmission electron microscopy (TEM) images were obtained on finely powdered samples using a Tecnai™ G2 F30 S-TWIN high resolution transmission electron microscope from FEI Company (Hillsboro, OR, USA) equipped with SAED. The microscope operated in transmission mode at 300 kV with TEM point resolution of 2 Å and line resolution of 1 Å. The nanospheres were dispersed into pure ethanol and ultrasonicated for 15 min. After that, diluted sample was poured onto a holey carbon-coated copper grid and left to dry before TEM analysis.

#### 4.3.3. SEM

SEM analysis was performed on a FEI electron microscope (FEI, Hillsboro, OR, USA), using secondary electron beams with energies of 30 keV, on samples covered with a thin gold layer.

#### 4.3.4. IR

IR mappings were recorded on a Nicolet iN10 MX FT-IR Microscope (Nicolet, Waltham, MA, USA) with MCT liquid nitrogen cooled detector in the measurement range  $4000$ – $700$   $\text{cm}^{-1}$ . Spectral collection was made in reflection mode at  $4$   $\text{cm}^{-1}$  resolution. For each spectrum, 32 scans were co-added and converted to absorbance using Omnic Picta software (Version 8.0, Thermo Scientific, Waltham, MA, USA, 2015). Approximately 250 spectra were analyzed for each sample. One absorption peak known as being characteristics for the prepared material was selected as spectral marker.

#### 4.3.5. Cell Viability

The CellTracker™ Red CMTPX (Promega, Madison, WI, USA) fluorescent dye has been designed to freely pass through cell membranes into cells, where it is transformed into cell-impermeant reaction products. CellTracker™ Red CMTPX dye is retained in living cells through several generations. The dye is transferred to daughter cells but not adjacent cells in a population. CellTracker™ Red CMTPX dye is designed to display fluorescence for at least 72 h and the dye exhibits ideal tracking properties: it is stable, nontoxic at working concentrations, well retained in cells, and brightly fluorescent at physiological pH. Red CMTPX was added to the cells at a concentration of 3  $\mu$ M and incubated for 30 min. The washed cells were analyzed under fluorescence microscope, having an emission spectrum in red (577/602 nm).

#### 4.3.6. *In Vivo* Biodistribution

The experimental protocol was applied according with the European Council Directive No. 86/609/24 November 1986, the European Convention on the Protection of Vertebrate Animals (2005) and the Romanian Government Ordinance No. 37/2 February 2002. The mice organs were collected under general anesthesia. Biological material was fixed, directly after the sampling, in 10% buffered neutral formalin, for 72 h, at room temperature, and then processed for routinely histological paraffin embedding technique. For the histological study of nanoparticles, 4- $\mu$ m thick serial sections were cut on a MICROM HM355s rotary microtome (MICROM International GmbH, Walldorf, Germany) equipped with a waterfall based section transfer system (STS, MICROM). The cross-sections were placed on histological blades treated with poly-L-Lysine (Sigma-Aldrich, Munich, Germany). After Hematoxylin-Eosin classical staining, cross-sections were evaluated and photographed using a Nikon Eclipse 55i light microscope equipped with a Nikon DS-Fi1 CCD high definition video camera (Nikon Instruments, Bucharest, Romania). Images were captured at  $\times$ 1000 magnification, stored and analyzed using Image ProPlus 7 AMS software (Media Cybernetics Inc., Marlow, Buckinghamshire, UK, 2015) [28,29].

#### 4.3.7. Biofilm Assay

The microbial strain used in this study *S. aureus* ATCC 25923 was obtained from the American Type Culture Collection (ATCC, Manassas, VA, USA). Fresh glycerol stocks were streaked on nutritive agar plates and colonies were allowed to develop for 24 h at 37 °C. Fresh colonies were used to obtain a bacterial suspension of a 0.5 McFarland (corresponding to  $1\text{--}3 \times 10^8$  CFU (colony form units)/mL) optical density in PBS. For assessing monospecific biofilm formation, 2 mL of nutritive broth were disposed in each well of a 6-wells plate, containing test (coated glass slides) and control (bare glass substrates) samples and seeded with the bacterial inoculum consisting of a volume of 20  $\mu$ L from the PBS bacterial suspension. After a period of 24 h incubation at 37 °C, the materials containing attached bacteria, were washed with PBS and transferred in a fresh well, containing 2 mL sterile nutritive broth and the incubation continued for another 24 h. The same procedure was repeated at 48 and 72 h, in order to assess the biofilm formation on the materials at different time intervals (24, 48 and 72 h). After each interval, the viable cell count (VCC) method was performed. For this, after each time point, biofilm embedded bacteria cells were detached by vigorous vortexing for 30 s. PBS suspensions containing detached bacteria cells were subjected to serial tenfold dilutions and each dilution was seeded on nutritive agar. Experiments were performed in triplicate and repeated on at least three separate occasions.

## 5. Conclusions

The antimicrobial activity results coupled with the good biocompatibility highlight the promising potential of the obtained coating based on magnetite and patchouli essential oil for the development

of novel bioactive wound dressings, as well as of other biomedical coatings or devices with tailored surface.

**Acknowledgments:** This work was supported by a grant of the Romanian National Authority for Scientific Research and Innovation, CNCS-UEFISCDI, project number PN-II-RU-TE-2014-4-2269. The SEM analyses on samples were possible due to EU-funding grant POSCCE-A2-O2.2.1-2013-1/Priority direction 2, Project No. 638/12.03.2014, cod SMIS-CSNR 48652.

**Author Contributions:** E.A., M.R., A.M.G., M.C. conceived the study; A.M.H., M.C.C., L.M., F.I., G.D.M., M.G., and A.M.G. drafted the manuscript together with E.A. and M.R. A.M.G., B.S.V., M.R. performed the synthesis and characterization of the samples. A.M.H., M.C.C., L.M., M.G., F.I. and G.M. performed the *in vitro* and *in vivo* experiments. A.M.G., M.C.C., M.R. and E.A. participated in the design of the study and coordination. All authors read and approved the final manuscript.

**Conflicts of Interest:** The authors declare no conflict of interest.

## References

1. Wolcott, R. Disrupting the biofilm matrix improves wound healing outcomes. *J. Wound Care* **2015**, *24*, 366–371. [[CrossRef](#)] [[PubMed](#)]
2. O'Meara, S.; Al-Kurdi, D.; Ologun, Y.; Ovington, L.G. Antibiotics and antiseptics for venous leg ulcers. *Cochrane Database Syst. Rev.* **2010**. [[CrossRef](#)]
3. Clinton, A.; Carter, T. Chronic wound biofilms: Pathogenesis and potential therapies. *Lab. Med.* **2015**, *46*, 277–284. [[CrossRef](#)] [[PubMed](#)]
4. Ammons, M.C. Anti-biofilm strategies and the need for innovations in wound care. *Recent Pat. Anti-Infect. Drug Discov.* **2010**, *5*, 10–17. [[CrossRef](#)]
5. Francolini, I.; Taresco, V.; Crisante, F.; Martinelli, A.; D'Ilario, L.; Ilario, L.; Piozzi, A. Water soluble usnic acid-polyacrylamide complexes with enhanced antimicrobial activity against staphylococcus epidermidis. *Int. J. Mol. Sci.* **2013**, *14*, 7356–7369. [[CrossRef](#)] [[PubMed](#)]
6. Ali, S.M.; Khan, A.A.; Ahmed, I.; Musaddiq, M.; Ahmed, K.S.; Polasa, H.; Rao, L.V.; Habibullah, C.M.; Sechi, L.A.; Ahmed, N. Antimicrobial activities of eugenol and cinnamaldehyde against the human gastric pathogen *Helicobacter pylori*. *Ann. Clin. Microbiol. Antimicrob.* **2005**, *4*, 1–7. [[CrossRef](#)] [[PubMed](#)]
7. Zhang, Z.; Vriesekoop, F.; Yuan, Q.; Liang, H. Effects of *nisin* on the antimicrobial activity of *d*-limonene and its nanoemulsion. *Food Chem.* **2014**, *150*, 307–312. [[CrossRef](#)] [[PubMed](#)]
8. Saviuc, C.M.; Drumea, V.; Olariu, L.; Chifiriuc, M.C.; Bezirtzoglou, E.; Lazar, V. Essential oils with microbicidal and antibiofilm activity. *Curr. Pharm. Biotechnol.* **2015**, *16*, 137–151. [[CrossRef](#)] [[PubMed](#)]
9. Freires, I.; Denny, C.; Benso, B.; de Alencar, S.; Rosalen, P. Antibacterial activity of essential oils and their isolated constituents against cariogenic bacteria: A systematic review. *Molecules* **2015**, *20*, 7329–7358. [[CrossRef](#)] [[PubMed](#)]
10. Bakkali, F.; Averbeck, S.; Averbeck, D.; Idaomar, M. Biological effects of essential oils—A review. *Food Chem. Toxicol.* **2008**, *46*, 446–475. [[CrossRef](#)] [[PubMed](#)]
11. Bilia, A.R.; Guccione, C.; Isacchi, B.; Righeschi, C.; Firenzuoli, F.; Bergonzi, M.C. Essential oils loaded in nanosystems: A developing strategy for a successful therapeutic approach. *Evid. Based Complement. Altern. Med.* **2014**, *2014*. [[CrossRef](#)] [[PubMed](#)]
12. Grumezescu, A.M.; Holban, A.M.; Andronescu, E.; Mogosanu, G.D.; Vasile, B.S.; Chifiriuc, M.C.; Lazar, V.; Andrei, E.; Constantinescu, A.; Maniu, H. Anionic polymers and 10 nm Fe<sub>3</sub>O<sub>4</sub>@UA wound dressings support human foetal stem cells normal development and exhibit great antimicrobial properties. *Int. J. Pharm.* **2014**, *463*, 146–154. [[CrossRef](#)] [[PubMed](#)]
13. Anghel, I.; Grumezescu, A.M.; Holban, A.M.; Ficai, A.; Anghel, A.G.; Chifiriuc, M.C. Biohybrid nanostructured iron oxide nanoparticles and *satureja hortensis* to prevent fungal biofilm development. *Int. J. Mol. Sci.* **2013**, *14*, 18110–18123. [[CrossRef](#)] [[PubMed](#)]
14. Anghel, I.; Holban, A.M.; Grumezescu, A.M.; Andronescu, E.; Ficai, A.; Anghel, A.G.; Maganu, M.; Laz, R.V.; Chifiriuc, M.C. Modified wound dressing with phyto-nanostructured coating to prevent *staphylococcal* and *pseudomonal* biofilm development. *Nanoscale Res. Lett.* **2012**, *7*. [[CrossRef](#)] [[PubMed](#)]

15. Anghel, I.; Grumezescu, A.M.; Andronescu, E.; Anghel, A.G.; Ficai, A.; Saviuc, C.; Grumezescu, V.; Vasile, B.S.; Chifiriuc, M.C. Magnetite nanoparticles for functionalized textile dressing to prevent fungal biofilms development. *Nanoscale Res. Lett.* **2012**, *7*. [[CrossRef](#)] [[PubMed](#)]
16. Boateng, J.; Catanzano, O. Advanced therapeutic dressings for effective wound healing—A review. *J. Pharm. Sci.* **2015**, *104*, 3653–3680. [[CrossRef](#)] [[PubMed](#)]
17. Kluytmans, J.; van Belkum, A.; Verbrugh, H. Nasal carriage of *Staphylococcus aureus*: Epidemiology, underlying mechanisms, and associated risks. *Clin. Microbiol. Rev.* **1997**, *10*, 505–520. [[PubMed](#)]
18. Archer, N.K.; Mazaitis, M.J.; Costerton, J.W.; Leid, J.G.; Powers, M.E.; Shirtliff, M.E. *Staphylococcus aureus* biofilms: Properties, regulation, and roles in human disease. *Virulence* **2011**, *2*, 445–459. [[CrossRef](#)] [[PubMed](#)]
19. Almeida, G.C.; dos Santos, M.M.; Lima, N.G.; Cidral, T.A.; Melo, M.C.; Lima, K.C. Prevalence and factors associated with wound colonization by *Staphylococcus* spp. And *Staphylococcus aureus* in hospitalized patients in inland northeastern brazil: A cross-sectional study. *BMC Infect. Dis.* **2014**, *14*. [[CrossRef](#)] [[PubMed](#)]
20. Anderson, D.J.; Kaye, K.S. *Staphylococcal* surgical site infections. *Infect. Dis. Clin. North Am.* **2009**, *23*, 53–72. [[CrossRef](#)] [[PubMed](#)]
21. Lima, A.F.; Costa, L.B.; Silva, J.L.; Maia, M.B.; Ximenes, E.C. Interventions for wound healing among diabetic patients infected with *Staphylococcus aureus*: A systematic review. *Sao Paulo Med. J.* **2011**, *129*, 165–170. [[CrossRef](#)] [[PubMed](#)]
22. Liakos, I.; Rizzello, L.; Scurr, D.J.; Pompa, P.P.; Bayer, I.S.; Athanassiou, A. All-natural composite wound dressing films of essential oils encapsulated in sodium alginate with antimicrobial properties. *Int. J. Pharm.* **2014**, *463*, 137–145. [[CrossRef](#)] [[PubMed](#)]
23. Sienkiewicz, M.; Łysakowska, M.; Pastuszka, M.; Bienias, W.; Kowalczyk, E. The potential of use basil and rosemary essential oils as effective antibacterial agents. *Molecules* **2013**, *18*, 9334–9351. [[CrossRef](#)] [[PubMed](#)]
24. Faoagali, J.; George, N.; Leditschke, J.F. Does tea tree oil have a place in the topical treatment of burns? *Burns* **1997**, *23*, 349–351. [[CrossRef](#)]
25. Sevgi, M.; Toklu, A.; Vecchio, D.; Hamblin, M.R. Topical antimicrobials for burn infections—An update. *Recent Pat. Anti-Infect. Drug Discov.* **2013**, *8*, 161–197. [[CrossRef](#)]
26. Yang, X.; Zhang, X.; Yang, S.P.; Liu, W.Q. Evaluation of the antibacterial activity of patchouli oil. *Iran. J. Pharm. Res.* **2013**, *12*, 307–316. [[PubMed](#)]
27. Grumezescu, A.; Gestal, M.; Holban, A.; Grumezescu, V.; Vasile, B.; Mogoantă, L.; Iordache, F.; Bleotu, C.; Mogoșanu, G. Biocompatible Fe<sub>3</sub>O<sub>4</sub> increases the efficacy of amoxicillin delivery against gram-positive and gram-negative bacteria. *Molecules* **2014**, *19*, 5013–5027. [[CrossRef](#)] [[PubMed](#)]
28. Fufa, M.O.; Mihaiescu, D.E.; Mogoanta, L.; Balseanu, T.A.; Mogosanu, G.D.; Grumezescu, A.M.; Bolocan, A. *In vivo* biodistribution of cnts using a balb/c mouse experimental model. *Rom. J. Morphol. Embryol.* **2015**, *56*, 1481–1493. [[PubMed](#)]
29. Istrate, C.M.; Holban, A.M.; Grumezescu, A.M.; Mogoanta, L.; Mogosanu, G.D.; Savopol, T.; Moisescu, M.; Iordache, M.; Vasile, B.S.; Kovacs, E. Iron oxide nanoparticles modulate the interaction of different antibiotics with cellular membranes. *Rom. J. Morphol. Embryol.* **2014**, *55*, 849–856. [[PubMed](#)]

